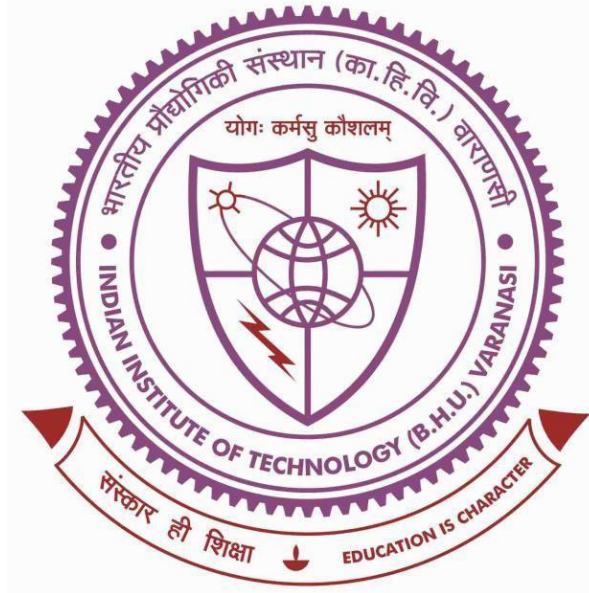




**Microstructure, Mechanical and Corrosion Behaviour  
of Indigenously Developed Carbide-free  
Nanostructured Bainitic Steel**




Thesis submitted in partial fulfilment for the  
Award of Degree

**Doctor of Philosophy**

By

**Sandeep Kumar Gupta**

DEPARTMENT OF METALLURGICAL ENGINEERING  
INDIAN INSTITUTE OF TECHNOLOGY  
(BANARAS HINDU UNIVERSITY)  
VARANASI-221005

17141009  


2023  




---

## CERTIFICATE

---

It is certified that the work contained in the thesis titled *“Microstructure, Mechanical and Corrosion Behaviour of Indigenously Developed Carbide-free Nanostructured Bainitic Steel”* by *Sandeep Kumar Gupta* has been carried out under my supervision and this work has not been submitted elsewhere for a degree.

*It is further certified that the student has fulfilled all the requirements of Comprehensive, Candidacy and SOTA for the award of Ph.D. degree.*



**Dr. Kausik Chattopadhyay**  
(Supervisor)

Department of Metallurgical Engineering  
Indian Institute of Technology  
(Banaras Hindu University)  
Varanasi-221005, India



**Dr. Rampada Manna**  
(Co-Supervisor)

Department of Metallurgical Engineering  
Indian Institute of Technology  
(Banaras Hindu University)  
Varanasi-221005, India



---

## DECLARATION BY THE CANDIDATE

---

I, *Sandeep Kumar Gupta*, certify that the work embodied in this thesis is my own bonafide work and carried out by me under the supervision of *Dr. Kausik Chattopadhyay* and *Dr. Rampada Manna* from *July 2017* to *July 2023*, at the *Department of Metallurgical Engineering*, Indian Institute of Technology (BHU), Varanasi. The matter embodied in this thesis has not been submitted for the award of any other degree/diploma. I declare that I have faithfully acknowledged and given credits to the research workers wherever their works have been cited in my work in this thesis. I further declare that I have not willfully copied any other's work, paragraphs, text, data, results, *etc.*, reported in journals, books, magazines, reports dissertations, theses, *etc.*, or available at websites and have not included them in this thesis and have not cited as my own work.

Date: 18 July, 2023


  
Sandeep Kumar Gupta

---


## CERTIFICATE BY THE SUPERVISORS

---

It is certified that the above statement made by the student is correct to the best of our knowledge.

  
**Dr. Kausik Chattopadhyay**  
(Supervisor)  
Department of Metallurgical Engineering  
Indian Institute of Technology  
(Banaras Hindu University)  
Varanasi-221005, India

  
**Dr. Rampada Manna**  
(Co-Supervisor)  
Department of Metallurgical Engineering  
Indian Institute of Technology  
(Banaras Hindu University)  
Varanasi-221005, India

  
**Prof. Sunil Mohan**  
(Head of the Department)  
Department of Metallurgical Engineering  
Indian Institute of Technology  
(Banaras Hindu University)  
Varanasi-221005, India



---

# COPYRIGHT TRANSFER CERTIFICATE

---

***Title of the Thesis:***

“Microstructure, Mechanical and Corrosion Behaviour of Indigenously Developed Carbide-free Nanostructured Bainitic Steel”

***Name of the Student:*** Mr. Sandeep Kumar Gupta

---

## COPYRIGHT TRANSFER

---

The undersigned hereby assigns to the Indian Institute of Technology (Banaras Hindu University) Varanasi all rights under copyright that may exist in and for the above thesis submitted for the award of the ***Ph.D. Degree.***



Date: 18 July, 2023

**Sandeep Kumar Gupta**

Place: Varanasi

**Note:** However, the author may reproduce or authorize others to reproduce material extracted verbatim from the thesis or derivative of the thesis for author's personal use provided that the source and the Institute's copyright notice are indicated.



*Dedicated*

*To*

*My Family*



---

## ACKNOWLEDGEMENTS

---

I take this opportunity to express my sincere thanks and gratitude to my supervisors, Dr. Kausik Chattopadhyay and Dr. Rampada Manna for their consistent help, encouragement and valuable discussions during the entire period of my research work. This thesis would not have been completed without their involvement and efforts. Because of their motivation I pursued my research problem. I consider myself extremely fortunate to have supervisors that genuinely cared about my work and responded to my queries timely. Besides my supervisors, I would like to express my deepest sense of gratitude to Prof. Vakil Singh for continuous help and inspiration throughout my research.

I am highly thankful to Prof. Sunil Mohan, Head of the Department and former Heads, Prof. N. K. Mukhopadhyay and Prof. R.K. Mandal for providing all the research facilities to successfully complete my research in the Department. Besides my supervisors I sincerely thank RPEC committee members: Prof. N. C. Santhi Srinivas, Department of Metallurgical Engineering and Dr. Meghanshu Vashista, Department of Mechanical Engineering, for their insightful comments and encouragement. I have deep sense of gratitude to Prof. O. P. Sinha, Dr. Sudipta Patra, Dr. Praveen Sathiyamoorthi, Dr. G.S. Mahobia, Dr. A.K. Mondal, Dr. J. K. Singh, Dr. Vikas Jindal and all other faculty members of the Department of Metallurgical Engineering, IIT (BHU), for their cooperation in testing and support during thesis work.

I am also thankful to Prof. I. Samajdar, Professor, IIT Bombay, for EBSD analysis. My sincere thanks to Dr. M. Z. Khan Yusufzai, Department of Mechanical Engineering, IIT(BHU) for important and valuable suggestions in my research work. My

special thanks to Prof. D. Chakraborty, Professor, IIT Kharagpur, for instrumented Charpy impact test.

My thanks to all my seniors Dr. Vaibhav Pandey, Dr. Yagnesh Shadangi, Dr. Asnit Gangwar, Dr. Avanish, Dr. Pramod Kumar, Dr. Prerna Mishra, Dr. Chandra Shekhar Kumar, Aman Laldas for their needful help. I am thankful to wonderful juniors and friends Dr. Jaydeep, Dr. Nitesh, Manik, Dr. Vineet, Dr. Shravan, Dr. Mudila Dhanunjaya Rao, Dr. Amit, Dr. Debabrat, Roopchand, Sarika, Ankit, Pawan, Manish, Vasu Shreyasi, Ishu, Ishwari, and others for their assistance and support. I am also thankful to all my junior students of M.Tech and Ph.D of our group from 2017 to 2023 for their constant support during experimental work.

I am also thankful to all the Lab and workshop staff specially, Shri Sushil Ji, Mr. Kamlesh Ji, Mr. Anjani Ji, Mr. Ramashrey Ji, Shri Lalit Kumar Singh Ji, Mr. Minz Ji, Mr. Balwant Ji, Mr. Mangal Ji and Mr. Deepak Ji for helping in preparation of fatigue and tensile samples. I would like to thank also, Patel Ji, Sushil Ji, Dubey Ji, Rana Ji, Rishabh Ji, Aamir Ji, Abtab Ji and all the other office and lab staff of the department. I would also like to extend my heartiest thanks to Prof. Rajiv Prakash (Prof. In-charge, CIFC) and Mr. Girish Sahu, Mr. Vinay and Mr. Nirmal Mallick for needful help in SEM, TEM and other research facilities.

I would like to acknowledge the Ministry of Human Resource and Development, Government of India for providing teaching assistantship during the entire period of my Ph.D. I would also like to acknowledge the Advanced Research Centre for Iron and Steel of the Institute, Steel Development Fund, Ministry of Steel, Government of India, under project No. 11(10)/SDF/2012-TW dated 14/03/2016 for JmatPro, vacuum induction melting furnace, X-ray diffraction scan and SERB, DST under the project no.

CRG/2019/000430 dated 02 March 2020 for EDM and electrochemical corrosion facility for the thesis work. Last, but not the least, I would like to express my deepest gratitude to my parents Late Shree Kapoor Chandra Gupta and Smt. Fulmati devi, my brothers Mr. Shradhey Gupta, Mr. Sanjay Gupta, Mr. Anuj Gupta, Mr. Dileep Gupta, Mr. Manoj Gupta, Mr. Neeraj Gupta and my sisters Mrs. Nitu Gupta, Mrs. Sangeeta Gupta, Mrs. Sadhana Gupta, Mrs. Soni Gupta, Mrs. Sunita Gupta, Mrs. Rupa Gupta, Mrs. Kiran Gupta and Ms. Pooja Gupta for their unconditional support and encouragement to pursue my interest.

I also wish to thank all my friends and the persons whose names have not been mentioned on this piece of paper for extending their cooperation directly or indirectly.

A rectangular box containing a handwritten signature in black ink that reads "Sandeep Kr. Gupta".

**SANDEEP KUMAR GUPTA**



---

## TABLE OF CONTENTS

---

LIST OF FIGURES .....	xix
LIST OF TABLES .....	xxxiii
ABBREVIATIONS .....	xxxv
SYMBOLS .....	xxxvii
PREFACE.....	xli
CHAPTER 1.....	1
INTRODUCTION AND LITERATURE REVIEW.....	1
1.1 INTRODUCTION .....	1
1.2 BRIEF HISTORY OF BAINITIC STEEL .....	2
1.2.1 Types of Bainite.....	3
1.2.2 T <sub>0</sub> Curve.....	6
1.2.3 Mechanism of Bainite Formation.....	8
1.3 MICROSTRUCTURE AND TENSILE BEHAVIOUR.....	12
1.4 LOW CYCLE FATIGUE BEHAVIOUR.....	19
1.5 IMPACT BEHAVIOUR .....	20
1.6 TRIBOLOGICAL BEHAVIOUR.....	21
1.7 CORROSION BEHAVIOUR.....	24
1.8 KNOWLEDGE GAPS .....	27
1.9 OBJECTIVES OF THE PRESENT INVESTIGATION .....	27
CHAPTER 2.....	29
MATERIALS AND EXPERIMENTAL METHODS.....	29
2.1 DESIGN OF THE MATERIALS .....	29
2.2 MATERIALS.....	30
2.2.1 Raw Materials.....	30
2.2.2 Melting and Casting .....	31
2.2.3 Calculations of Transformation Kinetics.....	34
2.2.4 Heat Treatment .....	38
2.3 MICROSTRUCTURAL CHARACTERIZATION .....	39
2.3.1 Optical Microscopy (OM) .....	39
2.3.2 Scanning Electron Microscopy (SEM).....	40
2.3.3 Transmission Electron Microscopy (TEM).....	41
2.3.4 X-ray Diffraction .....	41

2.4 MECHANICAL PROPERTIES.....	44
2.4.1 Hardness.....	44
2.4.2 Tensile Tests.....	45
2.4.3 Low Cycle Fatigue tests.....	45
2.5 CHARPY IMPACT TESTING.....	47
2.6 PIN-ON-DISC WEAR TESTING.....	48
2.7 CORROSION TESTING.....	49
2.7.1 Electrochemical Corrosion Tests.....	49
2.7.2 Static Immersion Corrosion Tests.....	51
CHAPTER 3.....	55
MICROSTRUCTURAL CHARACTERIZATION.....	55
3.1 OPTICAL MICROSTRUCTURE.....	55
3.2 X-RAY DIFFRACTION.....	57
3.3 SEM MICROSTRUCTURE.....	62
3.4 EBSD ANALYSIS.....	65
3.5 TEM MICROSTRUCTURE.....	72
3.6 DISCUSSION.....	77
3.7 CONCLUSIONS.....	80
CHAPTER 4.....	83
TENSILE BEHAVIOUR.....	83
4.1 HARDNESS.....	83
4.2 TENSILE BEHAVIOUR.....	84
4.3 TENSILE FRACTURE BEHAVIOUR.....	88
4.4 STRAIN-INDUCED MARTENSITIC TRANSFORMATION.....	91
4.4.1 X-Ray Diffraction Study of Tensile Tested Samples.....	91
4.4.2 EBSD analysis of Tensile Tested Samples.....	96
4.4.3 TEM Study of Tensile Tested Samples.....	100
4.5 WORK HARDENING BEHAVIOUR.....	103
4.6 DISCUSSION.....	116
4.6.1 Hardness and Tensile Behaviour.....	117
4.6.2 Work Hardening Behaviour.....	120
4.6.3 Tensile Fracture Behaviour.....	121
4.7 CONCLUSIONS.....	124
CHAPTER 5.....	127

FATIGUE AND CHARPY IMPACT BEHAVIOUR .....	127
5.1 LOW CYCLE FATIGUE BEHAVIOUR.....	127
5.1.1 Cyclic Stress Response.....	127
5.1.2 Fractography of the Fatigue Tested Sample .....	133
5.2 CHARPY IMPACT BEHAVIOUR .....	136
5.2.1 Fractography of the Charpy Impact Tested Sample .....	138
5.2.2 X-ray Diffraction Studies of Charpy Impact Tested Samples .....	140
5.3 DISCUSSION.....	141
5.3.1 Low Cycle Fatigue Behaviour.....	141
5.3.2 Charpy Impact Toughness .....	145
5.4 CONCLUSIONS .....	147
CHAPTER 6.....	149
TRIBOLOGICAL BEHAVIOUR.....	149
6.1 MASS LOSS .....	149
6.2 SPECIFIC WEAR RATE AND COEFFICIENT OF FRICTION.....	152
6.3 WORN SURFACE MORPHOLOGY AND EDS ANALYSIS .....	158
6.4 SURFACE ROUGHNESS MEASUREMENT .....	164
6.5 SUB-SURFACE MICROSTRUCTURAL CHARACTERIZATION BY TEM	168
6.6 STRAIN HARDENING EFFECTS .....	169
6.7 DISCUSSION.....	170
6.7.1 Tribological Behaviour.....	170
6.7.2 Wear Mechanism .....	173
6.8 CONCLUSIONS .....	174
CHAPTER 7.....	177
CORROSION BEHAVIOUR.....	177
7.1 ELECTROCHEMICAL CORROSION .....	177
7.1.1 Potentiodynamic Polarization Test .....	177
7.1.2 Electrochemical Impedance Spectroscopy (EIS) Test.....	179
7.1.3 Morphology of Corrosion Products After Electrochemical Test.....	182
7.2 IMMERSION TEST IN AQUEOUS 3.5% NaCl.....	183
7.2.1 Weight Loss Measurement .....	183
7.2.2 Morphology of Products of Corrosion After Immersion Test .....	185
7.3 DISCUSSION.....	190
7.3.1 EIS and Potentiodynamic Polarization.....	190

7.3.2 XPS Analysis .....	193
7.3.3 Corrosion Product Morphology After Electrochemical and Immersion Tests .....	206
7.3.4 Corrosion Mechanism.....	207
7.4 CONCLUSIONS.....	209
CHAPTER 8 .....	211
SUMMARY AND SUGGESTIONS FOR FUTURE WORK.....	211
8.1 SUMMARY .....	211
8.2 SUGGESTIONS FOR FUTURE WORK.....	213
REFERENCES.....	215
LIST OF PUBLICATIONS.....	235
.....	235
CONFERENCES PRESENTATIONS .....	235
NATIONAL / INTERNATIONAL WORKSHOP ATTENDED.....	235

---

## LIST OF FIGURES

---

<u>Figure No.</u>	<u>Figure Caption</u>	<u>Page No.</u>
<b>Figure 1.1</b>	Microstructures in a eutectoid steel. (a) Pearlite formed at 720°C (b) bainite formed at 290°C (c) bainite formed at 180°C (d) martensite [4].....	3
<b>Figure 1.2</b>	Time temperature transformation (TTT) diagram [17]. .....	4
<b>Figure 1.3</b>	Growth and development of upper or lower bainite [18].....	5
<b>Figure 1.4</b>	Transmission electron micrographs of bainite (a) upper bainite and (b) lower bainite [19]. .....	5
<b>Figure 1.5</b>	T <sub>0</sub> construction on the Fe-C phase diagram [30]. .....	8
<b>Figure 1.6</b>	Schematic illustration of structures produced by (a) diffusion-controlled growth, (b) and (c) repeated nucleation of sub-units which rapidly attain a limiting size, after Oblak and Hehemann [15].....	9
<b>Figure 1.7</b>	Schematic illustration of the morphology of the sheaf [33].....	10
<b>Figure 1.8</b>	Calculated phase fraction of cementite in equilibrium or para-equilibrium with austenite, in system Fe-Si-Mn-C with base composition Fe-1.2C-1.5Mn-1.5Si (wt-%) [34]. .....	11
<b>Figure 1.9</b>	Transmission electron micrograph of novel bainitic steel of composition Fe-0.98C-1.46Si-1.89Mn-0.26Mo-1.26Cr-0.09V austempered at 200°C for 5 days [35]. .....	12
<b>Figure 2.1</b>	Raw materials used for making studied compositions. ....	31
<b>Figure 2.2</b>	(a) Vacuum induction melting furnace and (b) copper mold. ....	32

<b>Figure 2.3</b> Cast ingot.....	32
<b>Figure 2.4</b> Heat-treatment cycles for homogenization and hot-rolling .....	33
<b>Figure 2.5</b> Homogenized samples vacuum sealed in quartz tube. ....	34
<b>Figure 2.6</b> Hot-rolled plate (~75% reduction).....	34
<b>Figure 2.7</b> Calculated time-temperature austenitization (TTA) diagrams (a) B12VA alloy, (b) B14VA alloy and (c) B15VA alloy steels using the JMatPro database. ....	35
<b>Figure 2.8</b> Calculated TTT diagram of the B12VA steel using JMatPro database for an austenite grain size of ASTM 8 and austenitizing temperature of 950°C. ....	35
<b>Figure 2.9</b> Calculated TTT diagram of the B14VA steel using JMatPro database for an austenite grain size of ASTM 8 and austenitizing temperature of 950°C. ....	36
<b>Figure 2.10</b> Calculated TTT diagram of the B15VA steel using JMatPro database for an austenite grain size of ASTM 8 and austenitizing temperature of 950°C. ....	36
<b>Figure 2.11</b> Austempering heat-treatment cycles of the hot-rolled steels. ....	38
<b>Figure 2.12</b> Patenting heat-treatment cycles of the hot-rolled steels. ....	39
<b>Figure 2.13</b> Geometry of the tensile sample (all dimensions in mm). ....	45
<b>Figure 2.14</b> Geometry of LCF test sample (all dimensions in mm). ....	46
<b>Figure 2.15</b> Triangular Waveform. ....	46
<b>Figure 2.16</b> Charpy impact samples as per ASTM E23-18 standard (all dimensions are in mm). ....	47
<b>Figure 2.17</b> Potentiostat with flat cell having three electrode system. ....	50
<b>Figure 2.18</b> (a) & (b) Static immersion corrosion tests in an aqueous 3.5% NaCl solution. .....	52

<b>Figure 3.1</b> Optical microstructure of the austempered (at 250°C) steels (a) B12VA-1, (b) B12VA-2, (c) B14VA-1, (d) B14VA-2, (e) B14VA-1, and (f) B15VA-2. ....	56
<b>Figure 3.2</b> Optical microstructure of the pearlitic steels at 550°C: (a) P12VA, (b) P14VA and (c) P15VA. ....	57
<b>Figure 3.3</b> X-ray diffraction patterns of the austempered steels : (a) B12VA-1, (b) B12VA-2, (c) B14VA-1, (d) B14VA-2, (e) B15VA-1 and (f) B15VA-2. Here $\alpha_b$ and $\gamma$ stand for bainite and retained austenite, respectively. ....	59
<b>Figure 3.4</b> X-ray diffraction patterns of the patented steel at 550°C: (a) P12VA, (b) P14VA, and (c) P15VA. Here, $\alpha$ and $\text{Fe}_3\text{C}$ stand for ferrite and cementite, respectively. ....	62
<b>Figure 3.5</b> SEM secondary electron images (SEIs) of the austempered (at 250°C) bainitic steel (a) B12VA-1, (b) B12VA-2, (c) B14VA-1, (d) B14VA-2, (e) B14VA-1, and (f) B15VA-2. Here $\alpha_b$ , $\gamma_B$ , and $\gamma_F$ stand for bainite, blocky retained austenite and filmy retained austenite, respectively.....	64
<b>Figure 3.6</b> SEM secondary electron images (SEIs) of the patented steel at 550°C: (a) P12VA, (b) P14VA, and (c) P15VA. Here P stands for pearlite.....	65
<b>Figure 3.7</b> EBSD phase map of the austempered steel: (a) B12VA-1, (b) B12VA-2, (c) B14VA-1, (d) B14VA-2, (e) B15VA-1 and (d) B15VA-2. ....	66
<b>Figure 3.8</b> Image quality maps of the austempered samples along with LAGB and HAGB: (a) B12VA-1, (b) B12VA-2, (c) B14VA-1, (d) B14VA-2, (e) B15VA-1 and (f) B15VA-2, respectively. Fraction of the LAGB and HAGB are shown in insets. ....	67

**Figure 3.9** Inverse pole figure (IPF) map of normal direction of the sample, B12VA-1: (a) bainite, (b) austenite, B12VA-2: (c) bainite and (d) austenite. Colour codes of IPF maps for bainite and austenite are shown in the insets of Figure 3.8c & d. ....68

**Figure 3.10** Inverse pole figure (IPF) maps of normal direction of the austempered B14VA-1: (a) bainite, (b) IPF of austenite, B14VA-2: (c) bainite and (d) austenite. Colour codes of IPF maps for bainite and austenite are in the inset of Figure 3.10c & d. ....69

**Figure 3.11** Inverse pole figure (IPF) maps of normal direction of the austempered B12VA-1: (a) bainite, (b) austenite, B12VA-2: (c) bainite and (d) austenite. Colour codes of IPF maps for bainite and austenite are shown in the inset of Figure 3.10c & d. ....70

**Figure 3.12** KAM maps of the austempered samples: (a) B12VA-1, (b) B12VA-2, (c) B14VA-1, (d) B14VA-2, (e) B15VA-1 and (d) B15VA-2.....71

**Figure 3.13** TEM bright-field images(BFIs) of the austempered ( at 250°C) steels (a) B12VA-1, (b) B12VA-2, (c) B14VA-1, (d) B14VA-2, (e) B15VA-1, and (f) B15VA-2. Here  $\alpha_b$ ,  $\Upsilon_B$ , and  $\Upsilon_F$ , signify bainite, blocky retained austenite, and filmy retained austenite, respectively. ....73

**Figure 3.14** TEM micrographs of B12VA-2 (a) BFI, (a') magnified BFI inset, (b) SADP, (c) DFI from intense spot of (200)  $\Upsilon$ , and (d) DFI from less intense spot of (200)  $\alpha_b$ . ....74

**Figure 3.15** TEM bright-field images(BFIs) of (a)B15VA-1 and (b) B15VA-2. SAEDPs are inserted in the corresponding BFI.....75

<b>Figure 3.16</b> TEM bright-field images(BFIs) of pearlitic steel patented at 550°C: (a) P12VA, (b) P14VA, and (c) P15VA. Here P, Fe <sub>3</sub> C and α signify pearlite, cementite and ferrite, respectively. ....	76
<b>Figure 3.17</b> TEM micrographs of pearlitic steel (a) BFI of P15VA sample, a selected area in BFI marked by yellow square box is used for SADP and corresponding (b) SADP of P15VA. In this indexed pattern yellow net of spots indicates for pearlitic ferrite and red coloured net is for pearlitic cementite. ....	77
<b>Figure 4.1</b> Variation of Vickers hardness measured at 10 kgf of austempered and patented steels. ....	84
<b>Figure 4.2</b> Engineering stress-strain curves of austempered steels: B12VA-1, B12VA-2, B14VA-1, B14VA-2, B15VA-1 and B15VA-2 and patented steels: P12VA, P14VA and P15VA. ....	86
<b>Figure 4.3</b> True stress-true strain curves of austempered samples. Number 1-3 on the graph indicates the change in slope of the work hardening rate. ....	88
<b>Figure 4.4</b> SEM fractographs of samples austempered at 250°C (a) B12VA-1', (b) B12VA-2', (c) B14VA-1', (d) B14VA-2', (e) B15VA-1' and (f) B15VA-2', respectively. ....	90
<b>Figure 4.5</b> SEM fractographs of samples patented at 550°C (a) P12VA', (b) P14VA' and (c) P15VA', respectively. ....	91
<b>Figure 4.6</b> X-ray diffraction patterns of tensile fractured samples: (a) B12VA-1', (b) B12VA-2', (c) B14VA-1' and (d) B14VA-2'. ....	93
<b>Figure 4.7</b> X-ray diffraction patterns of the austempered and the tensile fractured samples: (a) B15VA-1, (b) B15VA-2, (c) B15VA-1' and (d) B15VA-2'. ....	94

**Figure 4.8** EBSD phase map of the tensile tested austempered steel: (a) B12VA-1', (b) B12VA-2', (c) B14VA-1', (d) B14VA-2', (e) B15VA-1' and (f) B15VA-2'. .....97

**Figure 4.9** KAM maps of the tensile tested austempered steel: (a) B12VA-1', (b) B12VA-2', (c) B14VA-1', (d) B14VA-2', (e) B15VA-1' and (f) B15VA-2'. .....97

**Figure 4.10** Image quality maps of the tensile fractured austempered samples along with LAGB and HAGB: (a) B12VA-1', (b) B12VA-2', (c) B14VA-1', (d) B14VA-2', (e) B15VA-1' and (f) B15VA-2', respectively. Fraction of the LAGB and HAGB are shown in insets. ....99

**Figure 4.11** TEM bright-field images (BFI) of tensile fractured samples (a)B12VA-1', (b) B12VA-2', (c) B14VA-1' and (d) B14VA-2' sample. SAED pattern and martensites are shown as magnified insets. ....101

**Figure 4.12** TEM bright-field images (BFI) of tensile fractured samples (a)B15VA-1', (b) B15VA-2', corresponding (c) BFI of B15VA-1' and (d) SAED pattern of B15VA-1' sample. Martensites are shown as magnified insets. ....102

**Figure 4.13** Logarithmic (base 10) true stress vs. logarithmic true plastic strain plots of (a) B12VA-1 and (b) B12VA-2 steels with respective fitting curves. ....107

**Figure 4.14** Logarithmic (base 10) true stress vs. logarithmic true plastic strain plots of (a) B14VA-1 and (b) B14VA-2 steels with respective fitting curves. ....108

**Figure 4.15** Logarithmic (base 10) true stress vs. logarithmic true plastic strain plots of (a) B15VA-1 and (b) B15VA-2 steels with respective fitting curves. ....110

**Figure 4.16** Variation of work hardening rate ( $\theta$ ) with the true stress: (a) B12VA-1 & B12VA-2, and (b) B14VA-1 & B14VA-2 samples. ....114

<b>Figure 4.17</b> Variation of logarithmic work hardening rate ( $\theta$ ) with the logarithm of the sum of the true pre-strain and true strain for B15VA-1 and B15VA-2 samples....	115
<b>Figure 5.1</b> Cyclic stress response of austempered samples B12VA-2.....	128
<b>Figure 5.2</b> Cyclic stress response of austempered sample B14VA-2. ....	129
<b>Figure 5.3</b> Cyclic stress response of austempered sample B15VA-2. ....	130
<b>Figure 5.4</b> Fatigue life cycles for the austempered steel samples B12VA-2, B14VA-2 and B15VA-2 at different total strain amplitudes. ....	131
<b>Figure 5.5</b> Coffin-Manson plots of the austempered samples B12VA-2, B14VA-2 and B15VA-2. ....	132
<b>Figure 5.6</b> SEM fractographs showing the fracture surface tested at strain amplitude of $\pm 0.50\%$ (a) B12VA-2, (b) B14VA-2 and (c) B15VA-2. (d), (e) and (f) reveals the magnified images of red color rectangle of (a), (b) and (c), respectively. ....	134
<b>Figure 5.7</b> SEM fractographs showing the fracture surface tested at strain amplitude of $\pm 0.80\%$ (a) B12VA-2, (b) B14VA-2 and (c) B15VA-2. (d), (e) and (f) reveals the magnified images of red color rectangle of (a), (b) and (c), respectively. ....	135
<b>Figure 5.8</b> X-ray diffraction studies of fatigue tested samples.....	136
<b>Figure 5.9</b> Variation of Charpy impact energy of austempered steels B12VA-1, B12VA-2, B14VA-1, B14VA-2, B15VA-1 and B15VA-2 with temperature.....	137
<b>Figure 5.10</b> Fractographs of the Charpy impact tested austempered steels at room temperature: (a) B12VA-1, (b) B12VA-2, (c) B14VA-1, (d) B14VA-2, € B15VA-1 and (f) B15VA-2.....	139

**Figure 5.11** Fractographs of the Charpy impact tested austempered steels at -40°C: (a) B12VA-1, (b) B12VA-2, (c) B14VA-1, (d) B14VA-2, (e) B15VA-1 and (f) B15VA-2. ....140

**Figure 5.12** X-ray diffraction pattern of the Charpy impact tested austempered samples: (a) B12VA-2, (b) B12VA-2, (c) B14VA-2, (d) B14VA-2, (e) B15VA-1 and (f) B15VA-2. ....141

**Figure 6.1** Variation of mass loss vs sliding distances at different normal loads: (a) B12VA-1, (b) B12VA-2, and (c) P12VA. ....150

**Figure 6.2** Variation of mass loss vs sliding distances at different normal loads: (a) B14VA-1, (b) B14VA-2, and (c) P14VA. ....151

**Figure 6.3** Variation of mass loss vs sliding distances at different normal loads: (a) B15VA-1, (b) B15VA-2, and (c) P15VA. ....152

**Figure 6.4** Variation of specific wear rate versus sliding distance for B12VA-1, B12VA-2 and P12VA at various applied loads: (a) 10 N, (b) 30 N, and (c) 50 N. ....153

**Figure 6.5** Variation of specific wear rate versus sliding distance for B14VA-1, B14VA-2 and P14VA at various applied loads: (a) 10 N, (b) 30 N, and (c) 50 N. ....154

**Figure 6.6** Variation of specific wear rate versus sliding distance for B15VA-1, B15VA-2 and P15VA at various applied loads: (a) 10 N, (b) 30 N, and (c) 50 N. ....155

**Figure 6.7** The fluctuation of CoF with sliding time for (a) B14VA-1, (b) B14VA-2, and (c) P14VA under varying normal loads. ....157

**Figure 6.8** The fluctuation in CoF with sliding time for (a) B14VA-1, (b) B14VA-2, and (c) P14VA under varying normal loads. ....157

**Figure 6.9** The fluctuation in CoF with sliding time for (a) B15VA-1, (b) B15VA-2, and (c) P15VA under varying normal loads..... 158

**Figure 6.10** SEM SEIs of worn surfaces after 6000m of sliding against tungsten carbide rotating disc at different loads, 10, 30 and 50 N, respectively: (a), (b) &(c) for B12VA-1, (d) (e) & (f) for B12VA-2 and (g), (h) & (i) for P12VA samples..... 159

**Figure 6.11** SEM SEIs of worn surfaces after 6000m of sliding against tungsten carbide rotating disc at different loads, 10, 30 and 50 N, respectively: (a), (b) &(c) for B14VA-1, (d) (e) & (f) for B14VA-2 and (g), (h) & (i) for P14VA samples..... 160

**Figure 6.12** SEM SEIs of worn surfaces after 6000m of sliding against tungsten carbide rotating disc at different loads, 10, 30 and 50 N, respectively: (a), (b) &(c) for B15VA-1, (d) (e) & (f) for B15VA-2 and (g), (h) & (i) for P15VA samples..... 162

**Figure 6.13** Energy dispersive spectroscopy analysis of worn surfaces after 6000m of sliding against tungsten carbide rotating disc at loads of 10, 30 and 50 N, respectively: (a), (b) &(c) for B15VA-1, (d), (e) &(f) for B15VA-2 and (g), (h) & (i) for P15VA..... 163

**Figure 6.14** SEM energy dispersive spectroscopy analysis of wear debris after sliding distance of 6000 m at 50 N load (a) SEM SEI of B15VA-2, (b) EDS analysis of marked region 1, (c) EDS analysis of marked region 2, (d) SEM SEI of P15VA, (e) EDS analysis of marked region 3 and (f) EDS analysis of marked region 4..... 164

**Figure 6.15** AFM analysis of the worn surfaces after 6000m of sliding against tungsten carbide rotating disc at various loads of 10, 30 and 50 N, respectively: (a), (b) &(c) for B15VA-1, (d) (e) & (f) for B15VA-2 and (g), (h) & (i) for P15VA..... 165

<b>Figure 6.16</b> Variation of surface roughness of worn surfaces with sliding distance at different normal loads: (a) B12VA-1, (b) B12VA-2 and (c) P12VA. ....	166
<b>Figure 6.17</b> Variation of surface roughness of worn surfaces with sliding distance at different normal loads: (a) B14VA-1, (b) B14VA-2 and (c) P14VA. ....	167
<b>Figure 6.18</b> Variation of surface roughness of worn surfaces with sliding distance at different normal loads: (a) B15VA-1, (b) B15VA-2 and (c) P15VA. ....	168
<b>Figure 6.19</b> TEM BFI of sub-surface of the worn layer of B15VA-1. SAD pattern of the selected yellow coloured square area is depicted in inset. Here, $\epsilon_m$ , $\alpha_b$ and $\Upsilon_F$ denote epsilon martensite, bainite and filmy retained austenite, respectively. ....	169
<b>Figure 6.20</b> Microhardness variation with depth from the worn surfaces of austempered and patented samples after sliding distance of 6000 m at load of 50 N. ....	170
<b>Figure 6.21</b> Microstructure of cross-section of worn surface of the specimen by SEM (a) bainitic steel, B15VA-2 and (b) pearlitic steel, P15VA. Energy dispersive spectroscopy analysis of marked area are shown in insets. ....	172
<b>Figure 6.22</b> Schematic diagram showing wear mechanism in bainitic and pearlitic steels. ....	174
<b>Figure 7.1</b> Electrochemical potentiodynamic polarization curves (Tafel plots) of the bainitic and pearlitic steel samples (a) B12VA alloy: B12VA-1, B12VA-2 and P12VA, (b) B14VA alloy: B14VA-1, B14VA-2 and P14VA, and (c) B15VA alloy: B15VA-1, B15VA-2 and P15VA. ....	178
<b>Figure 7.2</b> Electrochemical impedance spectroscopy (EIS) plot of the austempered bainitic steel and pearlitic steel: (a) Nyquist plots, (b) Bode magnitude plots, (c)	

Bode phase plots, and (d) Fitted equivalent electrical circuit and its graphical representation. ....	180
<b>Figure 7.3</b> SEM secondary electron images (SEIs) of the corroded surfaces after electrochemical test of the austempered ( at 250°C) bainitic steel (a) B12VA-1, (b) B12VA-2, (d) B14VA-1, (e) B14VA-2, (g) B14VA-1, and (h) B15VA-2 and also, pearlitic steel (at 550°C): (c) P12VA, (f) P14VA, and (i) P15VA. ....	183
<b>Figure 7.4</b> Variation of the weight loss (mg/cm <sup>2</sup> ) of the bainitic and pearlitic steel samples during static immersion test. ....	184
<b>Figure 7.5</b> (a) variation of the corrosion rate (CR), charge transfer resistance (R <sub>ct</sub> ), and polarization resistance (R <sub>p</sub> ) obtained after the electrochemical test, (b) trends of corrosion rate after electrochemical and immersion test of the austempered bainitic steel and pearlitic steel samples .....	185
<b>Figure 7.6</b> SEM secondary electron images (SEIs) of the corroded surfaces after 30 days of immersion test of the austempered ( at 250°C) bainitic steel (a) B12VA-1, (b) B12VA-2, (d) B14VA-1, (e) B14VA-2, (g) B14VA-1, and (h) B15VA-2 and also, pearlitic steel (at 550°C): (c) P12VA, (f) P14VA, and (i) P15VA. ....	187
<b>Figure 7.7</b> Energy dispersive spectroscopy (EDS) of the corroded surfaces after 30 days immersion test of the austempered ( at 250°C) bainitic steel (a) B12VA-1, (b) B12VA-2, (d) B14VA-1, (e) B14VA-2, (g) B14VA-1, and (h) B15VA-2 and also, pearlitic steel (at 550°C): (c) P12VA, (f) P14VA, and (i) P15VA in aqueous 3.5% NaCl solution. ....	188
<b>Figure 7.8</b> SEM secondary electron images (SEIs) of the corroded surfaces after 30 days of immersion test of the Bainitic steel: (a) B15VA-2, (b) Magnified SEI of selected	

area of Figure 7.8(a) indicated by yellow rectangle, (c) EDS spectra of pink colour marked area, and (d) EDS spectra of pink colour marked area. Inset in Figure 7.8(b).

.....189

**Figure 7.9** SEM secondary electron images (SEIs) of the corroded surfaces after 30 days of immersion test of the pearlitic steel (at 550°C): (a) P15VA, (b) Magnified SEI of yellow colour rectangle area of Figure 7.9(a), (c) EDS spectra of pink colour marked area, and (d) EDS spectra of pink colour marked area. Inset Figure 7.9(b). .....190

**Figure 7.10** XPS survey spectrum of the corroded surfaces after 30 days immersion test of the austempered ( at 250°C) bainitic steels: B12VA-1, B12VA-2, B14VA-1, B14VA-2, B14VA-1, and B15VA-2 and also, pearlitic steel (at 550°C): P15VA. 193

**Figure 7.11** The XPS spectrograph's peak-fitting results of Fe 2p<sub>3/2</sub> after 30 days immersion test of the austempered ( at 250°C) bainitic steels samples: (a) B12VA-1, (b) B12VA-2, (c) B14VA-1, (d) B14VA-2, (e) B14VA-1, and (f) B15VA-2 and also, pearlitic steel (at 550°C): (g) P15VA. ....196

**Figure 7.12** The XPS spectrograph's peak-fitting results of O 1s after 30 days immersion test of the austempered ( at 250°C) bainitic steels samples: (a) B12VA-1, (b) B12VA-2, (c) B14VA-1, (d) B14VA-2, (e) B14VA-1, and (f) B15VA-2 and also, pearlitic steel (at 550°C) of (g) P15VA. ....197

**Figure 7.13** The XPS spectrograph's peak-fitting results of Cr 2p after 30 days immersion test of the austempered (at 250°C) bainitic steels samples: (a) B12VA-1, (b) B12VA-2, (c) B14VA-1, (d) B14VA-2, (e) B14VA-1, and (f) B15VA-2 and also, pearlitic steel sample (at 550°C): (g) P15VA in an aqueous 3.5% NaCl solution. ....198

**Figure 7.14** The XPS spectrograph's peak-fitting results of Co 2p after 30 days immersion test of the austempered ( at 250°C) bainitic steels samples: (a) B12VA-1, (b) B12VA-2, (c) B14VA-1, (d) B14VA-2, (e) B14VA-1, and (f) B15VA-2 and also, pearlitic steel (at 550°C): (g) P15VA in an aqueous 3.5% NaCl solution. .... 199

**Figure 7.15** The XPS spectrograph's peak-fitting results of Ni 3p<sub>3/2</sub> after 30 days immersion test of the austempered ( at 250°C) bainitic steels: (a) B15VA-1, (b) B15VA-2 and , pearlitic steel (at 550°C): (c) P15VA in an aqueous 3.5% NaCl solution..... 200

**Figure 7.16** The XPS spectrograph's peak-fitting results of Mo 3d<sub>3/2</sub> after 30 days immersion test of the austempered ( at 250°C) bainitic steels: (a) B12VA-1, (b) B12VA-2, (c) B14VA-1, (d) B14VA-2, (e) B14VA-1, and (f) B15VA-2 and also, pearlitic steel (at 550°C): (g) P15VA in an aqueous 3.5% NaCl solution. .... 201

**Figure 7.17** The XPS spectrograph's peak-fitting results of Al 2p<sub>3/2</sub> after 30 days immersion test of the austempered ( at 250°C) bainitic steels samples: (a) B12VA-1, (b) B12VA-2, (c) B14VA-1, (d) B14VA-2, (e) B14VA-1, and (f) B15VA-2 and also, pearlitic steel (at 550°C): (g) P15VA in an aqueous 3.5% NaCl solution. .... 203

**Figure 7.18** The XPS spectrograph's peak-fitting results of Mn 2p<sub>3/2</sub> after 30 days immersion test of the austempered ( at 250°C) bainitic steels samples: (a) B12VA-1, (b) B12VA-2, (c) B14VA-1, (d) B14VA-2, (e) B14VA-1, and (f) B15VA-2 and also, pearlitic steel (at 550°C): (g) P15VA in aqueous 3.5% NaCl solution. .... 204

**Figure 7.19** The XPS spectrograph's peak-fitting results of Si 2p<sub>3/2</sub> after 30 days immersion test of the austempered ( at 250°C) bainitic steels samples: (a) B12VA-1, (b) B12VA-2, (c) B14VA-1, (d) B14VA-2, (e) B14VA-1, and (f) B15VA-2 and also, pearlitic steel (at 550°C): (g) P15VA in aqueous 3.5% NaCl solution. .... 205

**Figure 7.20** The proposed corrosion mechanism for (a) pearlitic steel, (b) bainitic steel and (c) steel with high carbon.....208

**Figure 7.21** Cross-sectional microstructure of corroded samples by secondary electron imaging in SEM (a) pearlitic steel, P15VA and (b) bainitic steel, B15VA-2.....209

---

**LIST OF TABLES**

---

<u><b>Table No.</b></u>	<u><b>Table Caption</b></u>	<u><b>Page No.</b></u>
<b>Table 1.1</b>	Microstructure parameters and mechanical properties of nanostructured bainitic steels.....	17
<b>Table 2.1</b>	Selected compositions (by mass%).....	29
<b>Table 2.2</b>	Chemical composition of the raw materials (by mass%).....	30
<b>Table 2.3</b>	Chemical composition of hot-rolled steels (by mass%).....	33
<b>Table 2.4</b>	Transformation time for different fraction of bainite.....	38
<b>Table 2.5</b>	Test matrix for Low cycle fatigue tests.....	47
<b>Table 2.6</b>	Test parameters of tribological studies of austempered and patented steels.....	48
<b>Table 3.1</b>	Volume fraction of bainite and retained austenite, crystallite size (C.S.), lattice strain (L.S.), dislocation density ( $\rho$ ) and $C_Y$ of the austempered steels.....	60
<b>Table 3.2</b>	Microstructural features of austempered and patented steels.....	77
<b>Table 4.1</b>	Mechanical properties of austempered and patented steels.....	87
<b>Table 4.2</b>	Microstructural features of the tensile fractured austempered steel.....	96
<b>Table 4.3</b>	Work hardening parameters derived from Ludwigson relationship.....	106
<b>Table 4.4</b>	Work hardening parameters derived from Swift relationship.....	109
<b>Table 4.5</b>	Work hardening parameters of transition stress and work hardening rates.....	112

<b>Table 4.6</b> Work hardening parameters of different slopes, transition strains and work hardening rates .....	116
<b>Table 5.1</b> Low cycle fatigue data of austempered samples B12VA-2, B14VA-2 and B15VA-2 at different total strain amplitudes.....	131
<b>Table 5.2</b> Low cycle fatigue parameters calculated from Coffin-Manson plots of the austempered steels. ....	133
<b>Table 5.3</b> Charpy impact energy of the austempered steels. ....	138
<b>Table 6.1</b> Average value of coefficient of friction at different load. ....	158
<b>Table 7.1</b> Electrochemical potentiodynamic polarization parameter, resistance potential ( $R_p$ ) and corrosion rate (CR) of the austempered bainitic steel and patented pearlitic steel. ....	179
<b>Table 7.2</b> Parameters of the electrochemical impedance spectroscopy (EIS) of the austempered and patented steels.....	181
<b>Table 7.3</b> Weight loss measurement during immersion in 3.5% NaCl solution for 30 days and corrosion rate(CR) after 30 days of immersion test of the austempered bainitic and patented pearlitic steels.....	185

---

## ABBREVIATIONS

---

ASTM	American Society for Testing and Materials
BCC	Body Centred Cubic
CPE	Constant Phase Element
CR	Corrosion Rate
TRIP	Transformation Induced Plasticity
SIM	Strained-induced Martensite
EBS	Electron Back Scattered Diffraction
EDS/EDX	Energy Dispersive X-ray Spectroscopy
EIS	Electrochemical Impedance Spectroscopy
FCC	Face Centred Cubic
FESEM	Field Emission Scanning Electron Microscope
HCP	Hexagonal Closed Packing
HRTEM	High Resolution Transmission Electron Microscope
LCF	Low Cycle Fatigue
OCP	Open Circuit Potential
SAED	Selected Area Electron Diffraction
SEM	Scanning Electron Microscope
SEI	Secondary Electron Images
TEM	Transmission Electron Microscopy
BFI	Bright Field Images
DFI	Dark Field Images
XPS	X-Ray Photoelectron Spectroscopy
XRD	X-Ray Diffraction

IQ	Image Quality
IPF	Inverse Pole Figure
LAGB	Low Angle Grain Boundary
HAGB	High Angle Grain Boundary
KAM	Kernel Average Misorientation
YS	Yield Strength
UTS	Ultimate Tensile Strength
TE	Total Elongation
UE	Uniform Elongation
PSE	Product of Strength and Elongation

---

## SYMBOLS

---

$^{\circ}\text{C}$	Degree Centigrade
$\mu\text{m}$	Micrometre
$\text{nm}$	Nanometre
$\alpha$	Ferrite
$\alpha_{\text{b}}$	Bainite
$\alpha'$	Martensite
$\Upsilon$	Retained Austenite
$\Upsilon_{\text{F}}$	Filmy Retained Austenite
$\Upsilon_{\text{B}}$	Blocky Retained Austenite
$\text{P}$	Pearlite
$\blacklozenge$	Cementite
$V^{\circ}_{\text{RA}}$	Volume Fraction of Initial Retained Austenite
$V_{\text{RA}}$	Volume Fraction of Retained austenite After SIM Transformation
$V_{\text{B}}$	Volume Fraction of Bainite
$V_{\text{M}}$	Volume Fraction of Martensite
$\theta$	Theta
$C_{\Upsilon}$	Carbon Concentration in Retained Austenite
$\lambda$	Inter Lamellar Spacing
$\text{kHz}$	Kilo Hertz
$\text{mHz}$	Milli Hertz
$\text{mg}$	Milligram
$\text{mm}$	Millimetre

ml	Millilitre
$t_B$	Bainite plate thickness
$t_{RA}^F$	Thickness of Filmy Retained Austenite
$t_{RA}^B$	Size of Blocky Retained Austenite
a	Lattice Parameter
B	Crystallite Size
$k^\circ$	Scherrer Constant
cm	Centimetre
s	Second
$k'$	Constant
K	Strength coefficient
$K_1$	Strength coefficient
n	Strain Hardening Exponent
kN	kilo Newton
kV	kilo Volt
$\lambda$	Wavelength
$\varepsilon$	Root mean square of micro-strain
$\Delta\varepsilon_{t/2}$	Total strain amplitude
$\Delta\varepsilon_{p/2}$	Plastic strain amplitude
$\Delta\varepsilon_{e/2}$	Elastic strain amplitude
MPa	Mega Pascal
Ra	Average Surface Roughness
HV	Vickers hardness
$2N_f$	Number of reversals to failure

$\epsilon'_f$	Fatigue ductility coefficient
$I_{\text{corr}}$	Corrosion current
$E_{\text{corr}}$	Corrosion potential
$\beta_a$	Anodic Tafel slope
$\beta_c$	Cathodic Tafel slope
$\rho$	density
$E$	Elastic Modulus
$\mu\text{A}$	Microampere
$\Delta w$	Weight Loss
$t$	Immersion Period
$Z''$	Impedance Imaginary Component
$Z'$	Impedance Real Component



---

## PREFACE

---

Nanostructured bainitic steels represent a major advance in technology for producing very large quantities of three-dimensional objects like rail, armor, transmission shaft and bearing. The nanostructure bainitic steel usually is a mixture of slender plates of bainite embedded in a matrix of carbon enriched austenite. This austenite is stable under ambient conditions. Previous researchers found that nanostructured bainitic steel can be made carbide-free by adding sufficient amount of silicon concentration and by adding elements like Mn and Ni that increase the thermodynamic stability of the austenite at room temperature. However, that makes the transformation kinetics sluggish. Accelerated transformation of bainite can be obtained by adding small amount of Al and Co. The evaluation of nanostructured bainitic steel reports low toughness, reasonable fatigue, wear and corrosion resistance. Very less study is available on the effect of higher amount of retained austenite on tensile properties of high carbon carbide-free nanostructured bainitic steels. No study is available on the low cycle fatigue behaviour of high carbon carbide-free nanostructured bainitic steel. Tribological study at low and medium carbon bainitic steel shows that with increasing percentage of carbon wear resistance increases. However, there is hardly any literature on tribological behaviour of high carbon carbide-free nanostructured bainitic steels. There is no significant study available in literature on corrosion behaviour of high carbon carbide-free nanostructured bainitic steel with high amount of retained austenite as well as with variation of austempering time. Therefore, the objectives of the present investigation are to produce high carbon carbide-free nanostructured bainitic steel with improved strength, toughness, fatigue, wear and corrosion resistance.

The present thesis is divided into eight chapters.

**Chapter 1** accounts literature survey on synthesis and characterization of nanostructured bainite and its resultant mechanical properties like tensile, fatigue and wear behaviour and corrosion properties to find scientific gaps. Chapter ends with the objectives of the present investigation. The objectives of the present investigation are:

1. Design and characterization of ultrahigh strength carbide-free nanostructured bainitic (NSB) steel at lowest possible austempering temperature.
2. Ductilization, strengthening and toughening of the NSB steel.
3. Evaluation of low cycle fatigue behaviour of NSB steel.
4. To study the influence of microstructure and mechanical properties on dry sliding wear behaviour of nanostructured bainitic steel.
5. To study the effect of microstructure on Electrochemical and immersion Corrosion behaviour of nanostructured bainitic steel.

**Chapter 2** describes the design, synthesis and processing of materials and procedures of characterization of phases, microstructure, mechanical and corrosion properties. Three alloy compositions were designed using Jmat-pro database to get three different levels of martensite start temperature (much below room temperature, below room temperature and above room temperature). The selected compositions except manganese was melted in vacuum in an induction furnace at 1600°C. The temperature of melt was dropped to 1575°C and vacuum was replaced by argon atmosphere. Ferro-manganese and manganese were added to the melt. The homogeneous melt was maintained at 1550°C and was cast as plate in a copper mold. The cast materials were homogenized at 1200°C for 24 h in vacuum followed by furnace cooling. The homogenized plates were hot rolled

at 1050°C for 75% reduction in thickness and air cooled. The chemical analysis of hot-rolled plates was characterized by optical emission spectroscopy. The rolled sheets were austenitized at 950°C for 30 minutes. One set of austenitized samples was austempered at 250°C for different time periods to get required amount of bainite and another set of samples was patented at 550°C for 1 h for fully fine pearlitic structure. The austempered and patented steels are characterized by x-ray diffraction for phases and its quantification, crystallite size, micro strain, dislocation density and carbon content of retained austenite. Morphology and distribution of coarse phases were imaged in optical microscope. Scanning electron microscopy (SEM) was utilized for morphology of bainite, retained austenite, pearlite and size of blocky austenite. The chemical composition of phases was determined by EDS. Morphology, size and its distribution of bainite and filmy austenite, carbides if any were studied using transmission electron microscopy. Selected area diffraction patterns were analysed for confirmation of phases. Further hardness, tensile, Charpy impact toughness and low cycle fatigue testing were conducted on austempered steels. Also, dry sliding wear and corrosion behaviour of austempered steels were conducted and compared with patented steels of the same composition.

**Chapter 3** illustrates the synthesis and microstructural characterization of high carbon high silicon carbide-free nanostructured bainitic steel. XRD and TEM studies confirm that the investigated steels are carbide-free. Austempering of specially designed B12VA, B14VA, and B15VA steels at 250°C results in carbide-free nanostructured bainite with plate thickness in the range of 24-36 nm along with filmy and blocky retained austenite. For a given composition and austempering temperature, increasing austempering time increases volume fraction of bainite, increases amount of filmy austenite but decreases blocky retained austenite. Austempering of B12VA, B14VA and B15VA steels for a

respective optimized period of 96 h, 48 h and 50 h at 250°C temperature produces ~65 % bainite and ~35% retained austenite.

**Chapter 4** describes in detail the strengthening behaviour of high carbon high silicon carbide-free nanostructured bainitic steel. Yield strength of nanostructured bainite increases with increasing bainite content but ultimate tensile strength is mainly controlled by strain-induced martensite (SIM). Hardness of the austempered samples increases with increasing bainite content. XRD and TEM analysis confirmed that chemically stable but mechanically unstable blocky retained austenite undergo strain-induced martensitic transformation in all three compositions with decreasing order from B15VA, B14VA and B12VA as carbon percentage is in increasing order. SIM leads to high ductility with increasing strength and hardness. Among selected three compositions, B15VA-1 shows highest total elongation of 29.2%, Yield strength of 1281 MPa, highest ultimate tensile strength (UTS) of 1889 MPa, tensile toughness ( $U_T$ ) of 492 MJ/m<sup>3</sup>, hardness of 602 HV and product of strength and elongation (PSE) value of 55.16 GPa%. Work hardening behaviour of the selected nanostructured bainitic steel matches with the Swift model of three stages of deformation mechanism with increasing strain. Bainitic-austenitic steel of selected composition fails by mixed mode of fracture; however, the ductile fracture predominates.

**Chapter 5** describes the low cycle fatigue and Charpy impact behaviour of high carbon high silicon carbide-free nanostructured bainitic steel. The low cycle fatigue (LCF) tests were conducted at  $5 \times 10^{-3} \text{ s}^{-1}$  strain rate and  $\pm 0.50\%$ ,  $\pm 0.60\%$ ,  $\pm 0.70\%$  and  $\pm 0.80\%$  strain amplitudes. It was observed that fatigue life decreases with increasing strain amplitude. B15VA-2 steel revealed excellent fatigue life (11322 cycles) at strain amplitude of  $\pm 0.50\%$  amongst the studied steels (B12VA-2, B14VA-2 and B15VA-2). Cyclic

hardening was observed in all the strain amplitudes for all samples. XRD studies of fatigue tested samples reveal the formation of new phase, martensite. During cyclic loading, blocky retained austenite which is chemically stable but mechanically unstable, is transformed to martensite and contributed to cyclic hardening. The crack initiation takes place at the surface in all the fatigue tested samples. The striations are very fine and are visible on some transgranular facets of some samples. B15VA-1 and B15VA-2 samples reveal better impact energy among the studied steels (15-18 J/cm<sup>2</sup>). Charpy impact samples reveal typical quasicleavage fractography, indicating a specific pattern of fracture morphology. The crack propagation predominantly occurred through interlath cracking, suggesting a specific mechanism of crack growth within the material.

**Chapter 6** discusses the sliding wear behaviour of high carbon high silicon carbide-free nanostructured bainitic steel and compared it with that of patented steel. Patenting of the steels at 550°C results in a fine pearlitic structure. X-ray diffraction and transmission electron microscopy (TEM) were used to confirm the presence of nanostructured bainite and retained austenite in austempered steels, as well as ferrite and cementite in patented steels. In patented steels, the optical, scanning, and transmission electron microscopy revealed the presence of lamellar pearlite. The hardness and tensile strength of patented steels are much less than that of austempered steels. The mass loss is linearly dependent on the load and the specific wear rate as well as coefficient of friction decreases with the rise in load from 10 N to 50 N. The hardening volume of B15VA-1 sample is greater than that of B15VA-2 and P15VA, and it is mainly due to the transformation of blocky retained austenite to strain-induced martensite. The austempered and patented samples of B12VA and B14VA reveals similar trends but higher specific wear rate than the B15VA. The bainitic pins exhibited superior tribological response than the pearlitic one. SEM analysis

of worn surfaces confirmed that at lower load (10 N), abrasive wear occurs but at higher load (50 N), the wear mechanism changes to adhesive along with abrasive in bainitic steel and oxidative wear along with adhesive and abrasive wear in pearlitic steel.

**Chapter 7** discusses the effect of microstructure on electrochemical and immersion corrosion behaviour of high carbon high silicon carbide-free nanostructured bainitic steel and patented steel. Electrochemical and immersion corrosion tests are conducted in an aqueous 3.5% NaCl solution. The corroded surfaces are analysed with the scanning electron microscope (SEM) and X-ray photoelectron spectrometer (XPS). Corrosion resistance increases with increasing carbon percentage due to the formation of magnetite ( $\text{Fe}_3\text{O}_4$ ), provided the content of other alloying elements remains the same. The presence of Ni decreases corrosion rate significantly, i.e., enhances corrosion resistance, charge transfer resistance ( $R_{ct}$ ) and polarization resistance ( $R_p$ ). Reducing retained austenite in nanostructured steel decreases the corrosion rate due to the lesser area of galvanic couples and the formation of uniform, compact, and non-porous passive layer. The bainitic steel samples demonstrated superior corrosion resistance to that of the pearlitic steel due to lesser cell formation. The corrosion mechanisms of high-carbon bainitic and pearlitic steel are discussed.

**Chapter 8** presents major conclusions drawn from the present investigation along with suggestions for the future work.